Supporting Information for

Legionella pneumophila macrophage infectivity potentiator protein appendage domains modulate protein dynamics and inhibitor binding

Wiedemann, C.[1, #], Whittaker[2, #], J.J., Pérez Carrillo[1, #], V.H., Goretzki[1, 3], B., Dajka[4,5], M., Tebbe[1], F., Harder[1], J.-M., Krajczy, P.[6], R., Joseph[3, 4, 5], B., Hausch[6,7], F., Guskov[2], A., Hellmich[1, 3, *], U.A.

[1]Faculty of Chemistry and Earth Sciences, Institute of Organic Chemistry and Macromolecular Chemistry, Friedrich Schiller University Jena, Jena, Germany

[2]Groningen Institute for Biomolecular Sciences and Biotechnology, University of Groningen, 9747AG, Groningen, The Netherlands

[3]Center for Biomolecular Magnetic Resonance, Goethe-University, Frankfurt/Main, Germany

[4]Institute for Biophysics, Goethe-University, Frankfurt/Main, Germany

[5]Department of Physics, Freie Universität Berlin, Germany

[6]Department of Chemistry and Biochemistry Clemens-Schöpf-Institute, Technical University Darmstadt, Darmstadt, Germany

[7]Centre for Synthetic Biology, Technical University of Darmstadt, 64283 Darmstadt, Germany

*Correspondence to UAH: ute.hellmich@uni-jena.de

[#]These authors contributed equally: C.W., J.J.W., V.H.P.C.

Table S1: Data collection and refinement statistics (molecular replacement)

	***Lp*MIP$^{1-213}$**	***Lp*MIP$^{1-213}$ + JK095**	***Lp*MIP$^{100-213}$ + JK095**	***Lp*MIP$^{77-213}$ + JK095**	***Lp*MIP$^{77-213}$ + JK236**	***Tc*MIP + JK236**
PDB-ID	8BJC	8BJD	8BK6	8BK5	8BJE	8BK4
Wavelength	0.9763	0.9763	0.9763	0.9763	0.9763	0.9795
Resolution range	62.24 - 1.71 (1.772 - 1.71)	48.07 - 2.4 (2.486 - 2.4)	59.92 - 2.263 (2.344 - 2.263)	29.7 - 1.44 (1.492 - 1.44)	45.86 - 1.491 (1.544 - 1.49)	35.99 - 1.342 (1.39 - 1.342)
Space group	P 43 21 2	P 43 21 2	P 43 21 2	P 31 2 1	P 31 2 1	P 21 21 21
a, *b*, *c* (Å)	77.773 77.773 103.789	76.752 76.752 103.597	73.557 73.557 103.286	53.54 53.54 77.36	52.951 52.951 73.146	42.493 57.529 67.712
α, β, γ (°)	90, 90, 90	90, 90, 90	90, 90, 90	90, 90, 120	90, 90, 120	90, 90, 90
Unique reflections	19488 (241)	12644 (1218)	13801 (1344)	23619 (2330)	15279 (250)	28364 (209)
Completeness (%)	55.53 (7.00)	99.91 (99.75)	99.63 (99.18)	99.21 (98.69)	76.74 (12.73)	74.79 (5.62)
Mean I/sigma(I)	12.2(2.61)	11.1(2.10)	8.0	9.92(2.59)	15.33(2.04)	15.56(1.30)
Wilson B-factor	22.40	45.77	46.45	18.67	19.02	13.38
R-meas	0.09	0.06	0.06	0.07	0.08	0.08
CC1/2	93.3(24.0)	99.7(22.1)	98.5(32.3)	99.6(21.8)	99.1(27.7)	99.2(26.0)
Reflections used in refinement	19488 (241)	12642 (1218)	13760 (1334)	23616 (2330)	15273 (250)	28314 (209)
Reflections used for R-free	971 (16)	607 (56)	663 (53)	1137 (132)	745 (15)	1444 (10)
R-work	0.2455 (0.3083)	0.2357 (0.3254)	0.2856 (0.3866)	0.1838 (0.3227)	0.1975 (0.2236)	0.1968 (0.2986)
R-free	0.2943 (0.3324)	0.2898 (0.4187)	0.3242 (0.4791)	0.2227 (0.3722)	0.2332 (0.3624)	0.2205 (0.2814)
Number of non-hydrogen atoms	1742	1644	1784	1271	1122	1507
macromolecules	1554	1573	1684	1059	1020	1316
ligands	105	72	76	110	85	43
solvent	139	20	24	148	58	148
Protein residues	205	208	226	135	134	163
RMS(bonds)	0.006	0.008	0.011	0.009	0.017	0.006
RMS(angles)	0.96	1.14	1.69	1.11	1.69	0.92
Ramachandran favored (%)	98.03	95.63	93.69	97.74	96.21	99.38
Ramachandran allowed (%)	1.97	4.37	5.86	2.26	3.03	0.62
Ramachandran outliers (%)	0	0	0.45	0	0.76	0
Rotamer outliers (%)	0.59	1.16	8.51	0.84	0.88	0.72
Clashscore	6.78	7.35	17.23	3.53	5.62	4.10
Average B-factor	27.24	46.16	57.56	24.55	31.56	17.53
macromolecules	26.94	45.64	56.87	23.63	31.19	16.61
ligands	28.82	61.86	76.29	16.76	29.50	16.37
solvent	29.95	47.15	46.24	34.46	39.63	26.06

*Values in parentheses are for the highest resolution shell.

Table S2: Parameters for error estimation of the probability distributions obtained using Tikhonov regularization for full-length *Lp*MIP K80C. Validation was performed as featured in the DeerAnalysis2019 software package[1].

Sample	Error validation					Regularization parameter (α)
	dimensionality (*d*)		starting time window			
	range	steps	range (ns)	steps	T_{max} (µs)	
K80C	2.8-3.2	9	240-1000	11	5.36	1258
K80C + JK095	2.8-3.2	9	240-1000	11	4.86	1584
K80C + JK236	2.8-3.2	9	240-1000	11	4.38	1000

Table S3: SAXS data reporting table for full-length *Lp*MIP.

Sample details			
SAMPLE	*Lp*MIP *apo*	*Lp*MIP + JK095	*Lp*MIP + JK236
SASBDB Accession Codes	SASxxxx	SASxxxx	SASxxxx
Organism		*Legionella pneumophilia*	
NCBI protein accession ID		66489975	
(amino acid range)		1-213*	
SEC-SAXS buffer		20 mM Tris pH 7.5, 10 mM DTT	
NaCl concentration		150 mM	
Sample injection volume		45	
Sample injection conc.		10 mg/mL	
SEC column		S200 Increase 5/150	
SEC flow rate		0.3 ml/min	
SEC temperature		20 ºC	
Instrument details			
Instrument		EMBL P12 bioSAXS beam line, DESY, Hamburg	
Exposure time/# frames		0.25 s (2400)	
X-ray wavelength/energy		0.124 nm (9996.5 eV)	
Sample-to-detector distance		3 m	
Scattering intensity scale		Arbitrary unit, a.u.	
SEC-SAXS primary data processing		CHROMIXS (ATSAS 3.0.1)	
# frames used for averaging	90	78	77
Working s-range (nm^{-1})	0.03-7.43	0.03-7.43	0.03-7.43
Guinier analysis:			
Primary data analysis software		PRIMUS (ATSAS 3.0.1)	
Guinier I(0) (σ)	8491(8)	8031(10)	7835(8)
R_g (Guinier, nm) (σ)	3.13(0.01)	3.11(0.01)	3.04(0.01)
sR_g range	0.34-1.30	0.41-1.29	0.27-1.30
p(r) analysis:			
Method		GNOM 5	
I(0), POR (σ)	8526(7)	8068(9)	7686(8)
R_g (POR, nm) (σ)	3.17(0.1)	3.14(0.01)	3.07(0.01)
D_{max} (nm)	10.0	10.0	9.4
Quality of fit, CorMap P / χ^2	2.75E-04 / 1.04	6.7E-0.2 / 1.02	1.7E-0.2 / 1.00
Porod volume (nm^3)	66	62	63
Shape classification	flat	flat	flat
Molecular Weight analysis:			
MW, calculated from amino acid sequence, kDa	45.6 (dimer)	46.5 (dimer with 2x JK095)	46.5 (dimer with 2x JK236)
MW from SAXS data, kDa	41-46	44-48	46-49
Rigid body/Normal mode modelling:			
Method		SREFLEX (five individual fits)	
Symmetry	P1	P1	P1
Template	8BJC	8BJD	8BJC
Initial template fit, CorMap P / χ^2	3.10E-59 / 14.30	1.87E-63 / 16.28	7.73E-60 / 10.45
	6.76E-03 / 1.16	5.3E-05 / 1.30	2E-06 / 1.75
	2.56E-08 / 1.26	1.3E-05 / 1.37	7.99E-10 / 1.86
Final model fit, CorMap P / χ^2	1.24E-11 / 1.32	4.11E-07 / 1.38	7E-06 / 1.88
	4.23E-04 / 1.32	7.99E-10 / 1.39	8.22E-07 / 1.90
	1.60E-09 / 1.33	7.99E-10 / 1.42	4.11E-07 / 1.93

*The nomenclature for *Lp*MIP$^{1-213}$ used in this manuscript refers to the processed protein after cleavage of the N-terminal signal peptide comprising residues 1-20, which would be denoted as *Lp*MIP$^{21-233}$ according to the NCBI protein accession ID.

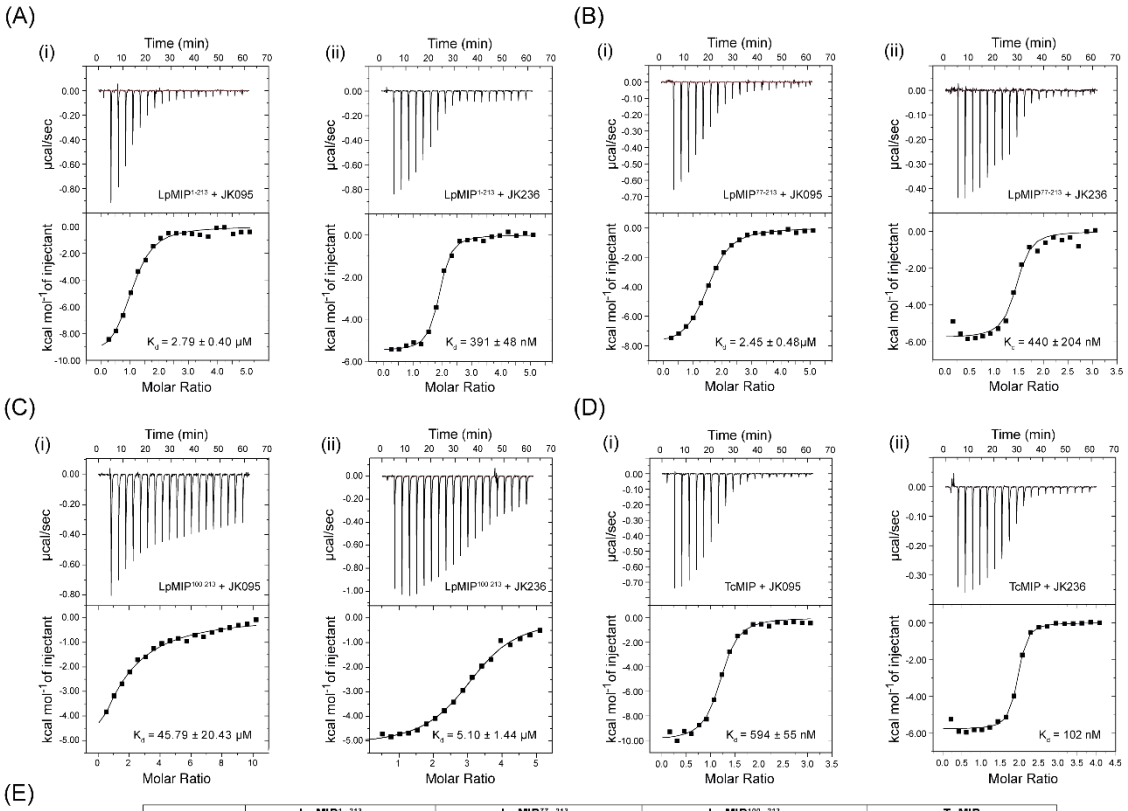

(E)

	LpMIP$^{1-213}$		LpMIP$^{77-213}$		LpMIP$^{100-213}$		TcMIP	
	+ JK095	+ JK236	+ JK095	+ JK236	+ JK095	+ JK236	+ JK095	+ JK236
Kd	2.79 ± 0.40 µM	391 ± 48 nM	2.45 ± 0.48 µM	440 ± 204 nM	45.79 ± 20.43 µM	5.10 ± 1.44 µM	594 ± 55 nM	150 ± 68 nM
ΔH (cal/mol)	-10045.5 ± 261	-5079.5 ± 592	-8673.5 ± 823	-5781.5 ± 0.7	-15060 ± 2941.56	-4587.5 ± 856.30	-9832 ± 251	-5940 ± 226
ΔS (cal/mol/deg)	-8.26 ± 1.15	12.3 ± 2.30	-3.40 ± 3.15	9.82 ± 0.97	-38.2	8.86 ± 3.44	-4.49 ± 0.66	11.4 ± 1.7
N	1.01 ± 0.04	2.01 ± 0.30	1.42 ± 0.11	1.76 ± 0.51	1.02 ± 0.26	2.79 ± 0.48	1.21 ± 0.06	1.94 ± 0.14

Fig. S1: Isothermal titration calorimetry of *Legionella pneumophila* and *Trypanosoma cruzi* MIP with bicyclic inhibitors. (A) *Lp*MIP$^{1-213}$ (full-length protein), **(B)** *Lp*MIP$^{77-213}$ and (**C**) *Lp*MIP$^{100-213}$ with JK095 and JK236 (i and ii, respectively). (**D**) *Tc*MIP with JK095 (i) and JK236 (ii). Representative ITC traces are shown, all measurements n=2. (**E**) Fitting parameters for ITC measurements.

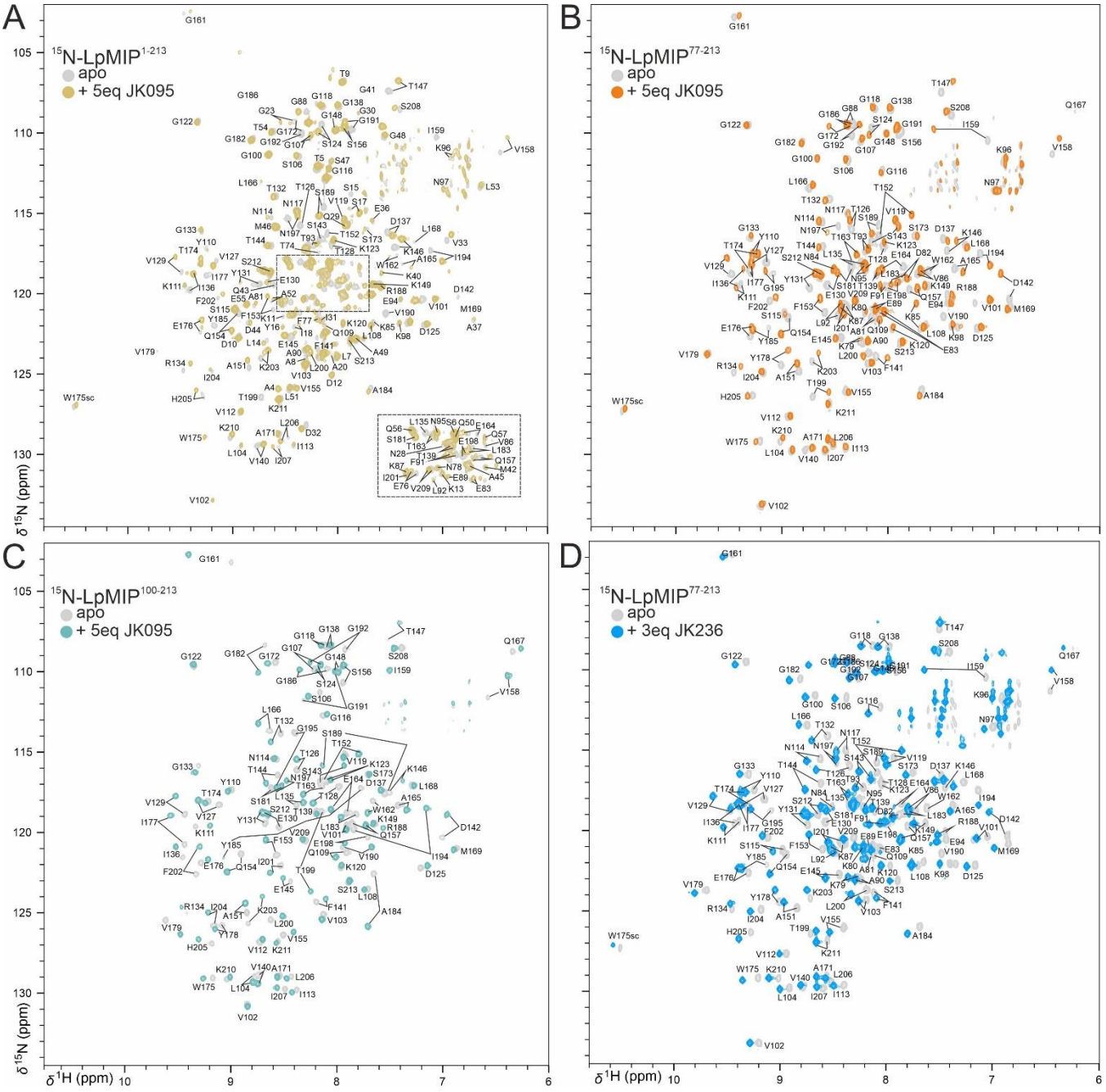

Fig. S2: Backbone NMR assignments of *Lp*MIP constructs in the apo and inhibitor bound states. Backbone assignments of (**A**) full-length *Lp*MIP without (grey) and with JK095 (sand), (**B**) *Lp*MIP$^{77\text{-}213}$ without (grey) and with JK095 (orange), (**C**) *Lp*MIP$^{100\text{-}213}$ without (grey) and with JK095 (teal), and (**D**) *Lp*MIP$^{77\text{-}213}$ without (grey) and with JK236 (blue). Previously published backbone amide resonance assignments for full-length *Lp*MIP (BMRB entry 7021) and *Lp*MIP$^{77\text{-}213}$ (BMRB entry 6334) could be partially transferred to our spectra and were verified using 3D assignment experiments under our buffer conditions. In contrast, the assignment of *Lp*MIP$^{100\text{-}213}$ had to be determined *de novo*, as the ^{1}H, ^{15}N-HSCQ spectrum of this construct differed significantly from the resonances of the FKBP domain in both *Lp*MIP$^{77\text{-}213}$ and full-length *Lp*MIP. The assignment for *Lp*MIP$^{100\text{-}213}$ has been deposited in the BMRB under accession number 51861.

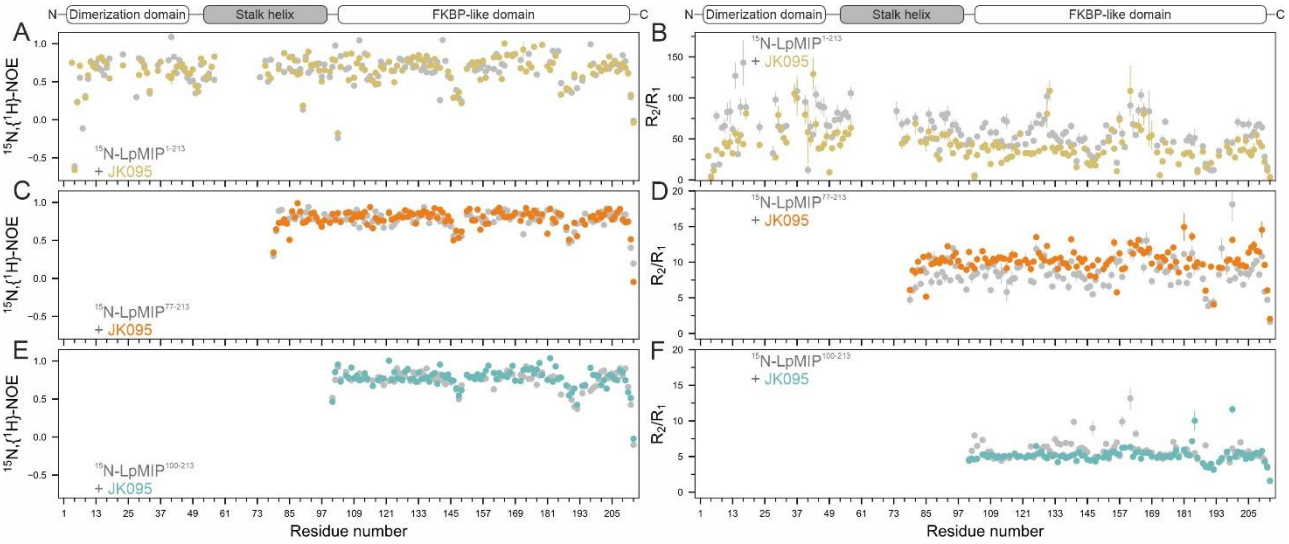

Fig. S3: Fast backbone dynamics of *Lp*MIP constructs in the absence and presence of JK095. ^{15}N, *{^{1}H}-NOE* and R_1/R_2 relaxation measurements of full-length *Lp*MIP (A, B), *Lp*MIP$^{77-213}$ (C, D) and *Lp*MIP$^{100-213}$ (E, F) without (grey circles) or in the presence of a five-fold molar excess of JK095 (colored circles).

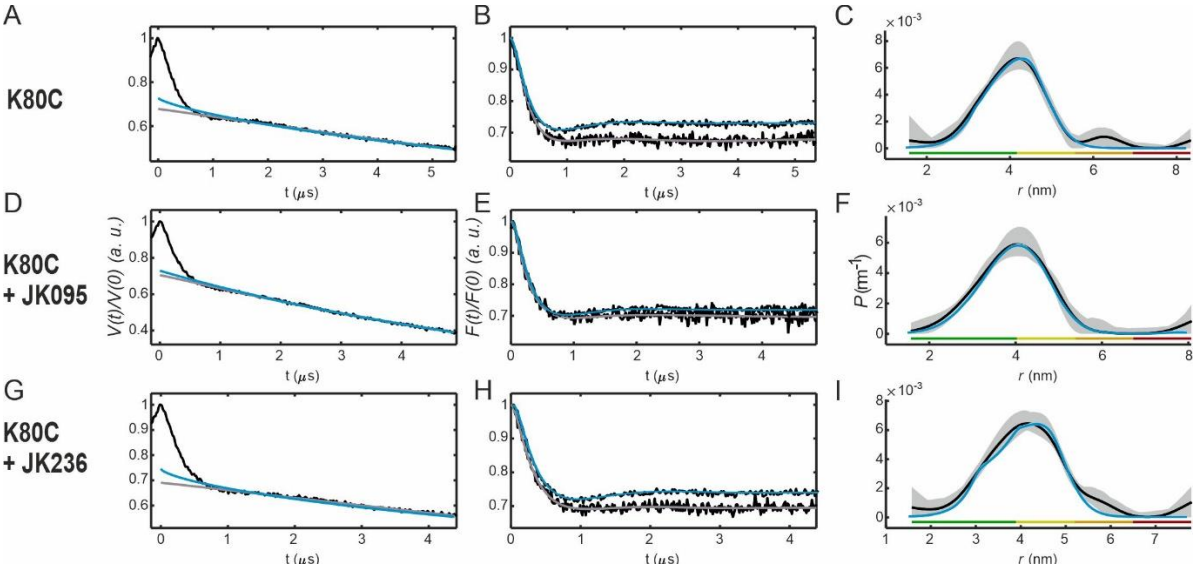

Fig. S4: PELDOR/DEER data analysis for *Lp*MIP K80C with the inhibitors JK095 and JK236. (A, D, G) The primary data (black) overlaid with the intermolecular (background) contribution from deep neural network analysis (blue) and Tikhonov regularization (grey). (B, E, H) The background corrected form factors overlaid with the fits. (C, F, I) The corresponding distance distributions.

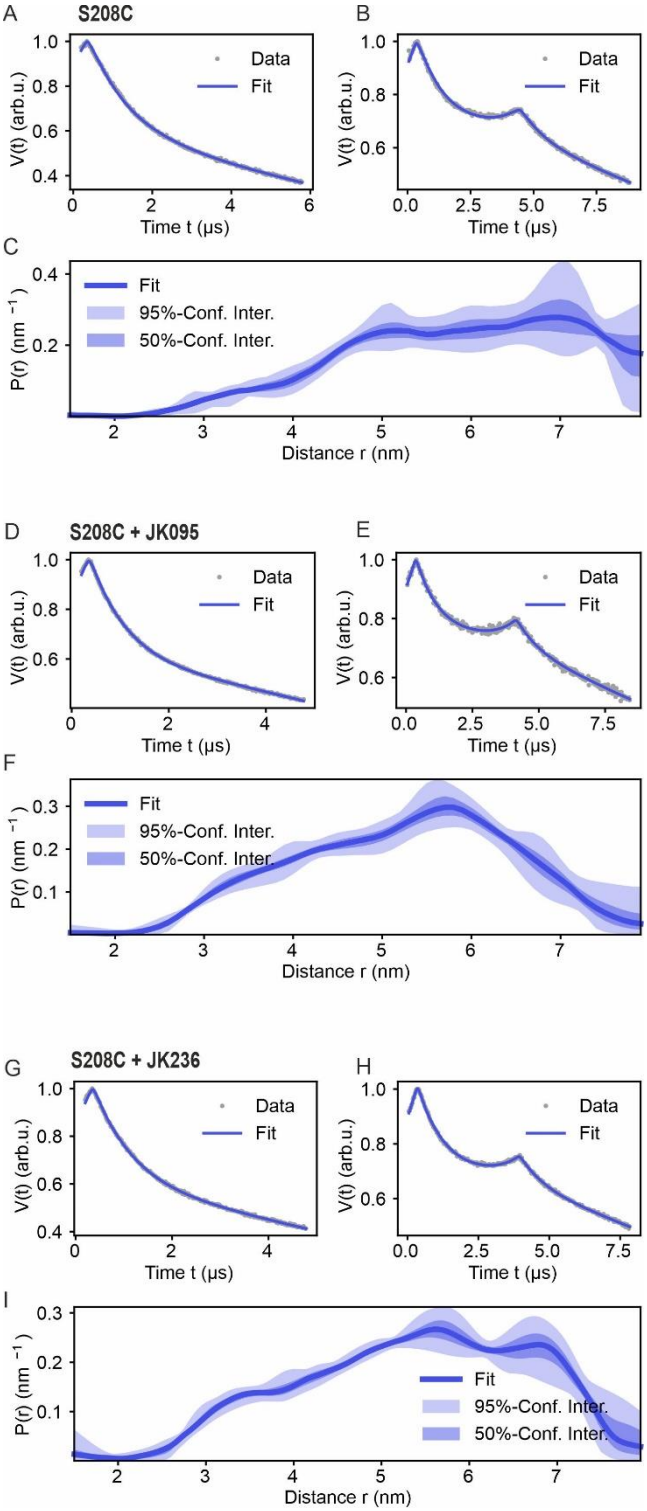

Fig. S5: PELDOR/DEER data analysis for *Lp*MIP S208C with the inhibitors JK095 and JK236. The 4-pulse and 5-pulse PELDOR data were globally analysed using the Python based DeerLab program. (A, D, G) The 4-pulse PELDOR data (grey) overlaid with the fit (blue). (B, E, H) The 5-pulse PELDOR data (grey) overlaid with the fit (blue); (C, F, I) The corresponding distance distributions with 50%- (shaded in dark blue) and 95% confidence intervals (shaded in light blue).

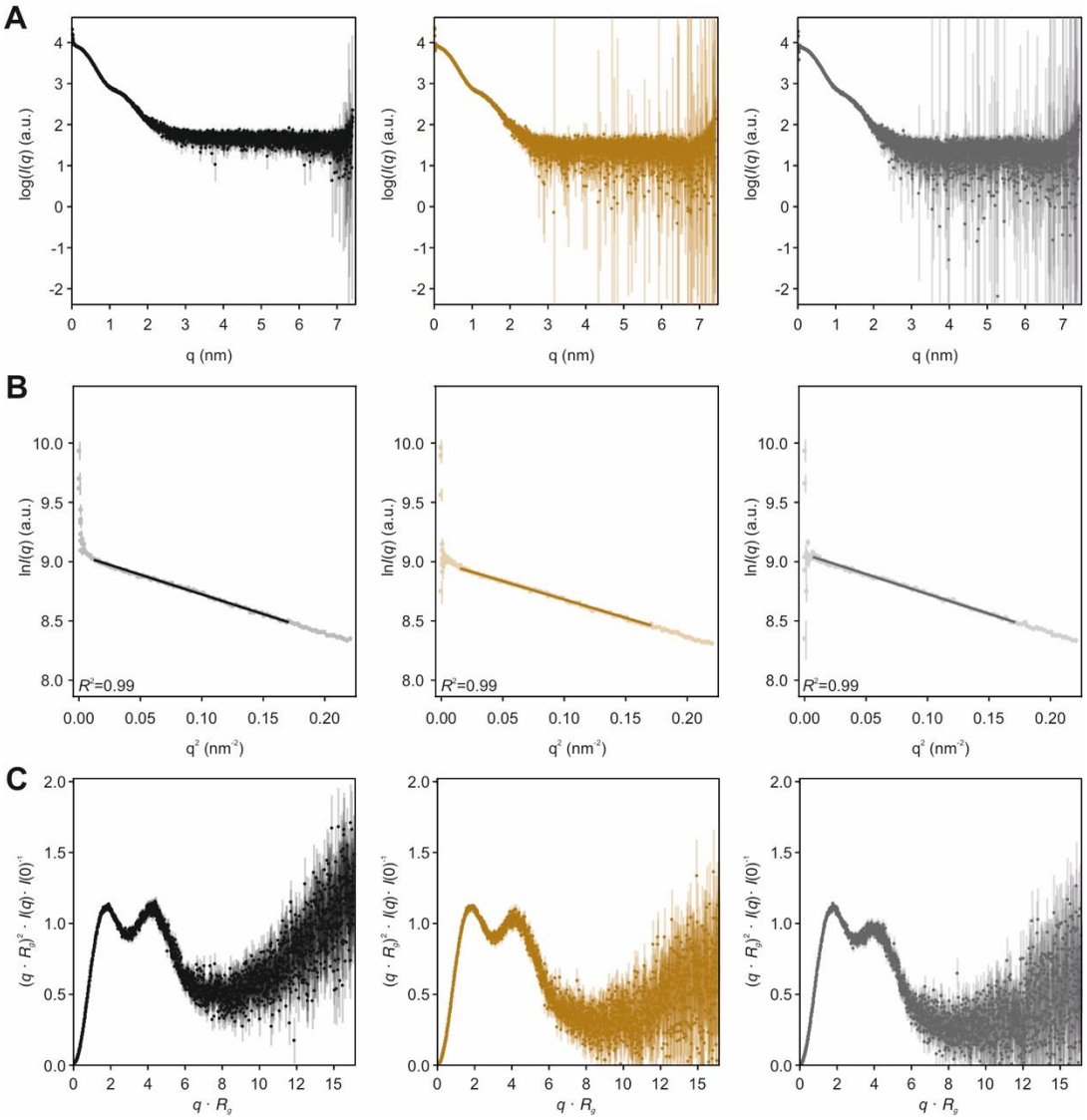

Fig. S6 – SAXS data collection of *Lp*MIP. (A) X-ray scattering profiles of *Lp*MIP apo (black), *Lp*MIP + JK095 (brown), and *Lp*MIP + JK236 (grey) plotted as the logarithm of the scattering intensity log($I(q)$) (a.u., arbitrary units) versus the momentum transfer, q. (B) Guinier-plots (ln$I(q)$ vs q^2, plotted to low-angle: $qR_g < 1.3$) of *Lp*MIP apo (black), *Lp*MIP + JK095 (brown), and *Lp*MIP + JK236 (grey). (C) Dimensionless Kratky-plots for *Lp*MIP apo (black), *Lp*MIP + JK095 (brown), and *Lp*MIP + JK236 (grey) plotted as $(qR_g)^2I(q)I(0)^{-1}$ vs. qR_g..

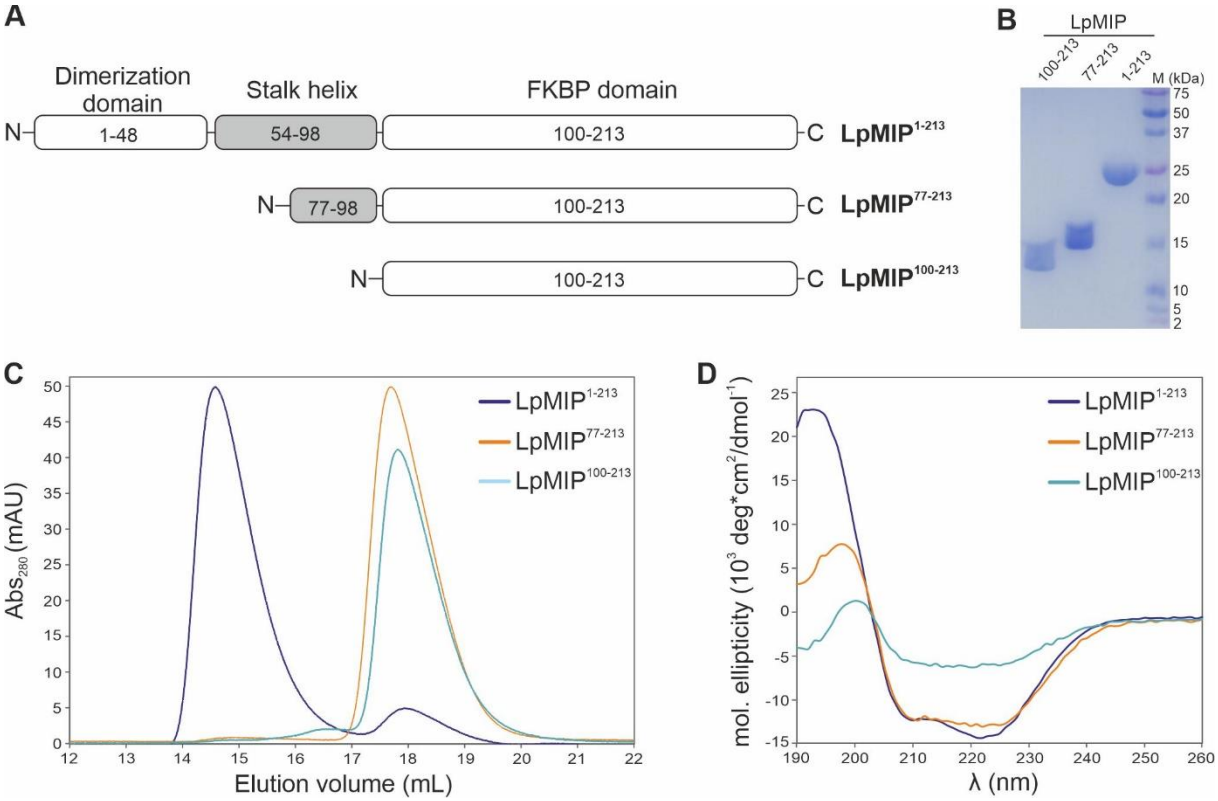

Fig. S7: Purification and structural integrity of *Legionella pneumophila* MIP deletion constructs. (**A**) Schematic of *Lp*MIP constructs used in this study. (**B**) SDS-PAGE of full-length *Lp*MIP (residues 1-213) and N-terminally truncated versions lacking the dimerization domain and half the stalk helix (*Lp*MIP$^{77\text{-}213}$) or the dimerization domain and the entire stalk helix (*Lp*MIP$^{100\text{-}213}$). (**C**) Analytical size exclusion chromatography of the three *Lp*MIP constructs. Note that *Lp*MIP$^{1\text{-}213}$ forms a dimer, while the two shorter constructs are monomeric. (**D**) Circular dichroism spectra of the three *Lp*MIP constructs displays the expected secondary structure content.

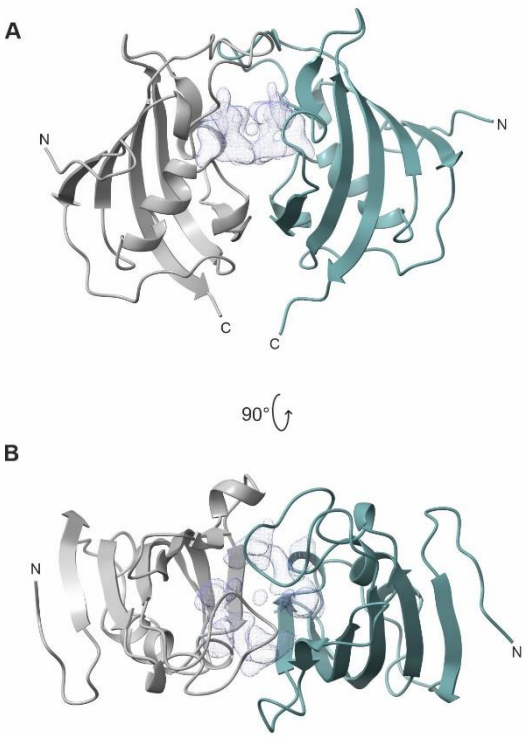

Fig. S8: *Lp*MIP$^{100\text{-}213}$ crystallizes as a dimer. In the crystal structure of *Lp*MIP$^{100\text{-}213}$ (PDB: 8BK6), the two protomers (grey, dark teal) in the unit cell align with an RMSD of 0.327 Å. The JK095 binding site cannot be defined clearly, instead there is density throughout the interface (light grey mesh). Of note, NMR spectroscopically derived rotation correlation times indicate that in solution, *Lp*MIP$^{100\text{-}213}$ is monomeric, irrespective whether JK095 is present or not (see main text for details).

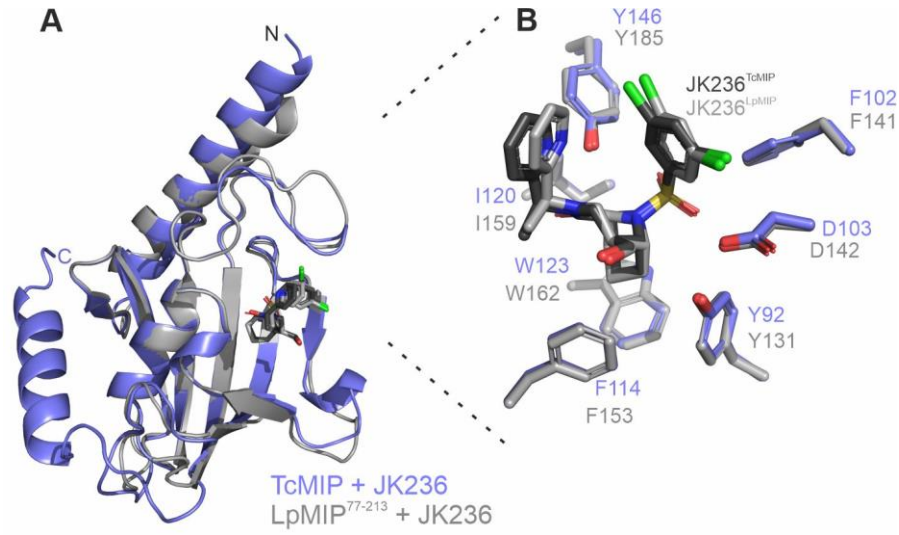

Fig. S9: Comparison of *Trypanosoma cruzi* and *Legionalla pneumophila* MIP in complex with a [4.3.1]-aza-bicyclic sulfonamide inhibitor. (**A**) Overlay of the X-ray structures of *Tc*MIP (blue) and *Lp*MIP$^{77\text{-}213}$ (grey) in complex with JK236 (PDB-IDs: 8BJE, 8BK4). Both structures align with a backbone RMSD of 0.51 Å. (**B**) Zoom into the binding site of *Tc*MIP and *Lp*MIP bound to JK236. Between JK236-bound *Tc*MIP and *Lp*MIP$^{77\text{-}213}$, the inhibitor binding stance is nearly identical and only a single rotamer of the hydroxymethyl group was observed. Likewise, the inhibitor's pyridine-linker methyl-group was solvent exposed in both proteins.

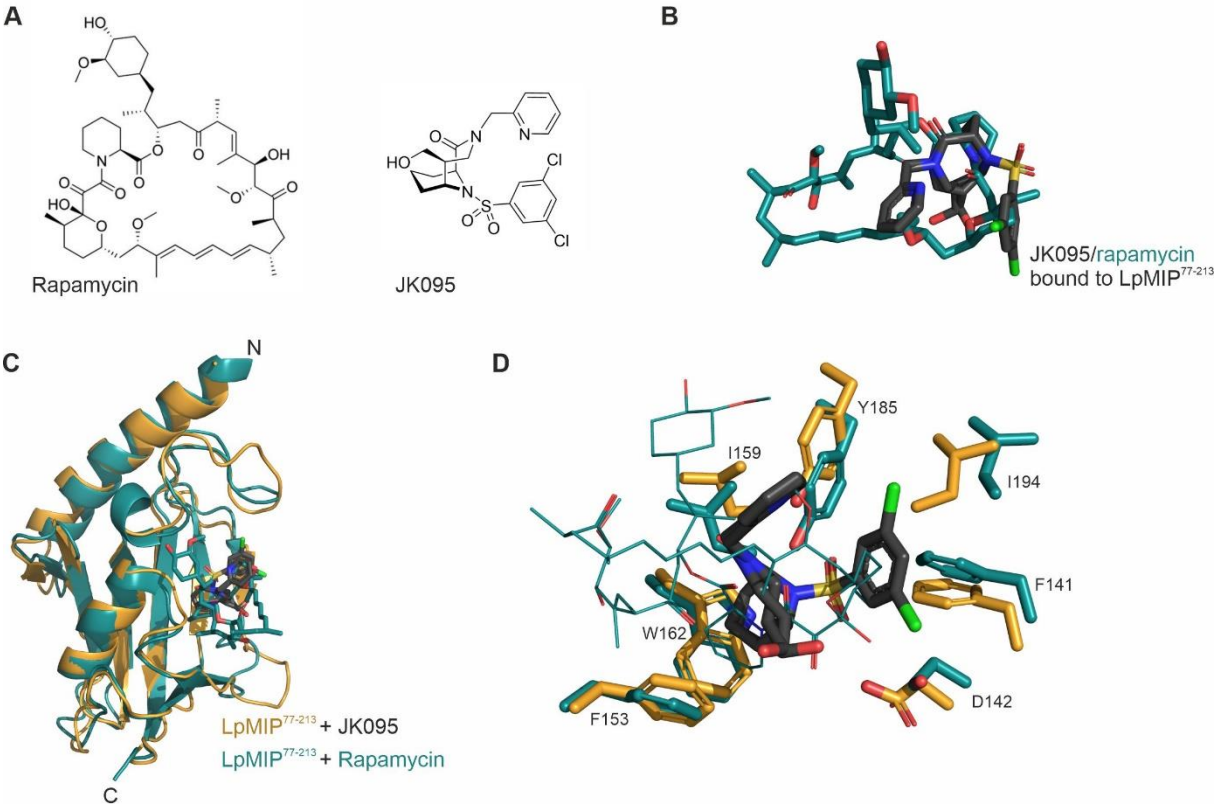

Fig. S10: Comparison of *Lp*MIP$^{77-213}$ bound to rapamycin or a bicyclic sulfonamide inhibitor. (**A**) Structures of rapamycin and JK095. (**B**) Overlay of rapamycin (dark teal) and JK095 (grey) bound to *Lp*MIP$^{77-213}$ (PDB IDs: 2VCD, 8BK5). (**C**) Overlay of *Lp*MIP$^{77-213}$ in complex with rapamycin (dark teal) or JK095 (orange, ligand shown in dark grey). (**D**) Zoom into the ligand binding site, residues important for ligand contacts are shown as sticks. For better visualization, rapamycin is shown with thin lines.

References for Supporting Information

1. Jeschke, G. *et al.* DeerAnalysis2006—a comprehensive software package for analyzing pulsed ELDOR data. *Appl. Magn. Reson.* **30**, 473–498 (2006).
2. Horstmann, M. *et al.* Letter to the Editor: 1H, 13C, 15N backbone and sidechain resonance assignment of Mip(77–213) the PPIase domain of the Legionella pneumophila Mip protein. *J Biomol NMR* **31**, 77–78 (2005).
3. Horstmann, M. *et al.* Domain Motions of the Mip Protein from Legionella pneumophila,. *Biochemistry* **45**, 12303–12311 (2006).
4. Fábregas Ibáñez, L., Jeschke, G. & Stoll, S. DeerLab: a comprehensive software package for analyzing dipolar electron paramagnetic resonance spectroscopy data. *Magnetic Resonance* **1**, 209–224 (2020).